УДК 551.463

Wave Chaos in Underwater Acoustics

Denis V. Makarov*
Leonid E. Kon'kov
Michael Yu. Uleysky
V. I. Il'ichev Pacific Oceanological Institute,
Baltiyskaya Str. 43, Vladivostok,
Russia

Received 10.04.2010, received in revised form 10.05.2010, accepted 10.06.2010

The problem of long-range sound propagation in an oceanic waveguide is considered. Even a weak range-dependent sound-speed perturbation is sufficient to cause chaotic dynamics in the ray limit. In the real ocean, an important role in the ray instability is played by small-scale depth oscillations of the sound-speed perturbation. Those small-scale oscillations should violate ray-wave correspondence. We carry out a comparative analysis of ray- and wave-based patterns in phase space and track how their discrepancies grow with decreasing the depth scale of a sound-speed perturbation. It is shown that the semiclassical theory can reproduce qualitative peculiarities of wave behavior even with small perturbation's scales. A strong conflict occurs only with very low acoustic frequencies.

Keywords: ray chaos, wave chaos, quantum chaos, long-range sound propagation, periodic orbits.

Introduction

The phenomenon of long-range sound propagation in the ocean, discovered in the middle of the XXth century [1–3], is still one of the main subjects of research in underwater acoustics. In the deep ocean, there is typically a minimum of the sound speed at some depth z_{a}. Up to this depth the sound speed decreases mainly due to decreasing of water temperature. Below z_{a} it increases due to hydrostatic pressure increases. The presence of the minimum of the sound speed leads to the formation of *an underwater sound channel* (USC). The depth z_{a}, where c is minimal, is referred to as the channel axis. According to the Snell's law, sound tends to propagate toward regions of lower speed, therefore, the sound speed profile $c(z)$ refracts waves toward the channel axis. Being trapped in the USC, the sound waves do not reach the lossy bottom and, therefore, they may propagate over long distances with relatively small attenuation.

When we study a wavefield pattern using the ray approximation, it is necessary to keep in mind the well-known fact that the ray approximation is just the short-wavelength limit of a wavefield, and its relevance demands a sound wavelength to be small compared with a length scale of ocean variability L, i. e.

$$\lambda_0 \ll L. \tag{1}$$

Typically, the deep ocean can be regarded as a stratified medium, and its variability in the horizontal direction is by $10^2 \div 10^3$ weaker than in the vertical one. The horizontal variability satisfies well the above condition, even for low sound frequencies of about 1 Hz. In the case of vertical variability, things are not so simple. The criterion (1) can be reformulated in terms of the transversal (vertical) acoustic wavenumber as

$$k_\perp = k_0 \sin\chi \gg L_z^{-1}, \tag{2}$$

*makarov@poi.dvo.ru

where L_z is a length scale of the vertical variability, $k_0 = 2\pi f/c_0$ is the wavenumber in the reference medium with $c = c_0$, f is a signal frequency, and χ is a grazing angle of a wave. Depth dependence of a sound speed can be expressed as a sum of two components. The first component slowly varies, resulting in forming an USC, and satisfies the condition (2) with sound frequencies of tens hertz and higher. The second one corresponds to small-scale variations mainly caused by high-number modes of an internal-wave field. If we deal with low-frequency signals, which are able to propagate over long distances, fulfillment of inequality (2) is very questionable. Although the second component has a significantly smaller amplitude than the first one, their contributions into a vertical gradient of the sound-speed can be comparable, especially in the neighborhood of the channel axis. As it was shown in [4,5], this circumstance results in strong chaos of near-axial rays. But, according to Eq. (2), ray approximation cannot be used for near-axial wavepackets, when $\sin\chi$ is close to zero.

On the other hand, as it was argued by Hegewisch, Cerruti and Tomsovic [6], small-scale features of a sound-speed profile should be irrelevant for refraction of waves with low frequencies, therefore, should be smoothed out in ray modeling. In particular, Hegewisch with coauthors showed that removing of features being smaller than some frequency-dependent threshold length scale doesn't alter a wavefield a lot, although these features enhance remarkably ray instability. Thus, we arrive at the intricate conflict of wave and ray descriptions: small-scale sound-speed variations give rise to strong ray chaos, but seem to be insignificant for wavefield evolution. So, there arise several important questions. What is the extent to which we can trust the ray approximation for low-frequency sound propagation? As rapid vertical oscillations of a sound-speed perturbation are an important source of ray chaos, do chaos-induced phenomena cease completely at low acoustic frequencies?

In the present paper we shall explore the differences between actual wavefields at various acoustic wavelengths and their ray-based counterparts. Also we shall track how those differences grow with decreasing depth scale of a sound-speed perturbation.

The paper is organized as follows. In the next section the model of a range-periodic waveguide is introduced. In Sec. 2, we describe shortly ray motion in this model, with the emphasis on the phenomenon of vertical resonance. Sec. 3 is devoted to manifestations of vertical resonance and other concomitant ray-based features in a structure of the Floquet modes. We finish with the summary of the results obtained.

1. The Model of a Waveguide

A sound-speed profile in the deep ocean can be represented as

$$c(z,r) = c_0 + \Delta c(z) + \delta c(z,r). \tag{3}$$

Typically, $|\delta c| \ll |\Delta c|$. In the present paper we consider the narrow–angle wave propagation, when the original Helmholtz equation for a wavefield reduces to the parabolic equation

$$\begin{aligned} &\frac{i}{k_0}\frac{\partial\phi(z,\,r)}{\partial r} = \hat{H}\phi(z,\,r), \\ &\hat{H} = -\frac{1}{2k_0^2}\frac{\partial^2}{\partial z^2} + U(z) + V(z,r), \\ &U(z) = \frac{\Delta c(z)}{c_0}, \quad V(z,r) = \frac{\delta c(z,r)}{c_0}. \end{aligned} \tag{4}$$

The parabolic equation formally coincides with the non-stationary Shrödinger equation. In this analogy, one treats range r as the time-like variable, $\Delta c(z)$ as an unperturbed potential, δc as a time-dependent perturbation, and k_0^{-1} as the Planck constant.

The model of a waveguide we use in numerical simulations is the biexponential model [7]

$$U(z) = \frac{b^2}{2}\left(e^{-az} - \eta\right)^2, \tag{5}$$

with an idealized model of the sound-speed perturbation

$$V(z,r) = \frac{\delta c}{c_0} = \varepsilon Y(z) \sin\frac{2\pi z}{\lambda_z} \sin\frac{2\pi r}{\lambda_r}, \quad \varepsilon \ll 1, \tag{6}$$

where the perturbation envelope $Y(z)$ is specified as

$$Y(z) = \frac{z}{B} e^{-2z/B}. \tag{7}$$

Formula (6) mimics a sound-speed perturbation caused by oceanic internal waves. Parameters of an unperturbed waveguide are fixed at the following values: $c_0 = 1480$ m/s, $a = 0.5$ km^{-1}, $b = 0.557$, $\eta = 0.6065$. The depth of the ocean bottom is 4 km.

2. Ray Dynamics

Here we shall describe briefly properties of ray dynamics. A more comprehensive analysis can be found in [8]. Ray trajectories obey the Hamiltonian equations

$$\frac{dz}{dr} = \frac{\partial H}{\partial p}, \quad \frac{dp}{dr} = -\frac{\partial H}{\partial z}, \tag{8}$$

with the Hamiltonian

$$H = \frac{p^2}{2} + U(z) + V(z,r). \tag{9}$$

Here p is a tangent of a ray grazing angle. The second equation in (8) can represented as

$$\frac{dp}{dr} = \frac{\varepsilon}{2}\left[k_z Y(\sin\Psi^- - \sin\Psi^+) - \frac{dY}{dz}(\cos\Psi^- - \cos\Psi^+)\right], \tag{10}$$

where $\Psi^\pm = k_z z \pm k_r r$, $k_z = 2\pi/\lambda_z$, $k_r = 2\pi/\lambda_r$. With low values of k_z, ray motion can be well described using the theory of nonlinear resonance [7,9,10]. In this case there arise chains of islands in phase space in the vicinities of ray-medium resonances determined by the condition

$$i\omega = jk_r, \tag{11}$$

where i and j are integers, ω is a spatial frequency of ray oscillations in a waveguide. Ray motion is predominantly stable unless the Chirikov's criterion [11]

$$\frac{\Delta\omega}{\delta\omega} \simeq 1 \tag{12}$$

is satisfied. Here $\Delta\omega$ and $\delta\omega$ are width of resonance (11) and distance between neighboring resonances in the ω-space, respectively. The criterion (12) means emergence of global ray diffusion in phase space due to the overlapping of resonances.

Since the formula (6) models an effect of internal oceanic waves, it is reasonable to assume that $k_z \gg |dY/dz|$. It implies rapid oscillations of the range-dependent term along a ray path, except for the resonant regions, where one of the following conditions, either

$$\frac{d\Psi^+}{dr} = k_z p + k_r \simeq 0, \tag{13}$$

or

$$\frac{d\Psi^-}{dr} = k_z p - k_r \simeq 0, \tag{14}$$

is fulfilled. Since these resonances are associated with ray motion with respect to the depth oscillations of the sound-speed perturbation, we shall refer to the resonances of this sort as vertical resonances. It can be shown that the strongest effect from vertical resonances is expected when (13) or (14) is satisfied near the channel axis (see [8] for details). Taking this into account, one can derive an unique condition

$$|p(z = z_\mathrm{a}, H)| \simeq \sqrt{2(H - U(z_\mathrm{a}))} = \frac{\lambda_z}{\lambda_r} \tag{15}$$

instead of the pair (13)–(14).

An important property of vertical resonances is that they cause ray chaos. Phase space location of the respective chaotic layer can be estimated using the formula (15). To illustrate that, we compute the Poincaré maps with various values of λ_z, while other parameters of the perturbation are fixed and specified as $\varepsilon = 0.005$, $B = 1$ km, $\lambda_z = 0.2$ km, $\lambda_r = 5$ km. The result of the computations is shown in Fig. 1. In the case of $\lambda_z = 2000$ m, the zone of vertical resonance lies outside the interval corresponding to rays propagating without reflections off the lossy bottom. Since that, ray motion is predominantly stable, as it is shown in the Poincaré map depicted in Fig. 1(a). Phase space of the ray equations contains a large central island of stability surrounded by the chaotic sea. There are several chains of ray-medium resonances inside the central island. The most prominent one corresponds to the ray-medium resonance 9 : 1, i. e. the resonance corresponding to $i = 9$ and $j = 1$ in Eq. (11). Other chains have remarkably smaller widths.

With decreasing λ_z twice, the condition (15) is fulfilled for steep rays with $|p(z_\mathrm{a})| \simeq 0.2$. This reduces considerably the area of the central island and destroys the ray-medium resonance 9 : 1 (see Fig. 1(b)). The ray-medium resonance 8 : 1, on the contrary, is enhanced. The respective chaotic layer is open, i. e. there are no barriers preventing rays from chaotic swinging and eventual reaching the attenuating bottom. This is an effect of ray escaping, causing additional transmission losses in long-range sound-propagation. As it was shown in [12], vertical resonance affecting steep rays causes especially strong losses due to ray escaping.

With $\lambda_z = 500$ m, the phase space pattern becomes especially non-trivial. As one can see in Fig. 1(c), there are two nested chaotic layers separated from each other by a narrow stripe of stability. The inner layer, occurred due to the vertical resonance with $|p(z_\mathrm{a})| \simeq 0.1$, contains numerous islands of stability within. An attentive view reveals that these islands belong to three chains, each of them consists of 8 islands. Such chains arise after bifurcations of periodic orbits which occur when the conditions (11) and (15) are fulfilled simultaneously, and k_z is large enough [8]. The outer layer is comparatively narrow and mainly caused by the contacts of ray-medium resonances with the degeneracy of ray oscillations, which is associated with non-monotonicity of the function $\omega(H)$ due reflections off the ocean surface.

The case of $\lambda_z = 200$ m is depicted in Fig. 1(d). The main peculiarity of this Poincaré map is the presence of a wide and almost uniform chaotic layer occupying the central domain of phase space and being surrounded by invariant curves. Another detail to be noted is that there is no remarkable islands inside the layer, except for the chain near the outer boundary. It implies almost ergodic ray diffusion inside the chaotic layer. Steeper rays are completely regular. This picture, i. e. chaos of near-axial rays and regularity of steeper ones, agrees good with experimental data on long-range sound propagation in the ocean (see, for instance, [13]). Thus, one can conclude that ray scattering on fast depth oscillations of the sound-speed perturbation is one of the main sources of ray chaos in underwater acoustics.

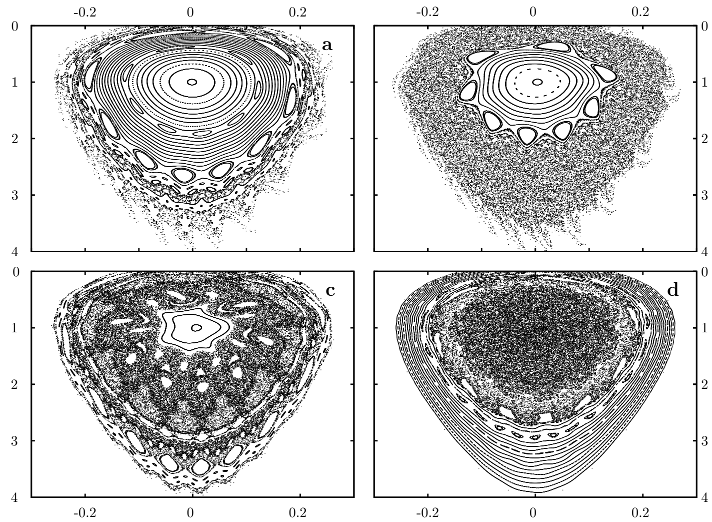

Fig. 1. Poincaré maps computed with $\lambda_z = 2000$ m (a), $\lambda_z = 1000$ m (b), $\lambda_z = 500$ m (c), and $\lambda_z = 200$ m (d)

3. Description of Wave Motion in Terms of the Floquet Modes

As Poincaré map serves as a convenient tool for exploring phase space patterns of ray motion in range-periodic waveguides, Floquet modes depicted via Husimi plots provide phase space representation of wave dynamics. The Floquet modes can be found by solving repeatedly the parabolic equation with different modes of the unperturbed waveguide as initial conditions, then constructing the Floquet matrix, and finding its eigenvectors which are namely the Floquet modes [14]. In this work the parabolic equation is solved numerically with the idealized boundary conditions

$$u|_{z=0} = 0, \quad \left.\frac{\partial u}{\partial z}\right|_{z=h} = 0, \tag{16}$$

where $h = 4$ km is the depth of the ocean bottom.

Four acoustic frequencies are considered: 20, 50, 100, and 200 Hz. Floquet modes are numbered in the order of increasing values of the parameter μ, defined as

$$\mu = \sum_m m|C_{mn}|^2, \tag{17}$$

where $\{C_{mn}\}$ are elements of the matrix with columns being the Floquet eigenvectors [14]. It allows one to find one-to-one correspondence between a Floquet mode and a corresponding phase-space region. Indeed, the value of μ can be related to a mean value of the action of the respective Floquet mode as

$$\mu \simeq k_0\langle I\rangle. \tag{18}$$

Phase-space representation of Floquet modes is obtained by means of the Husimi function which is proven as a suitable tool for this purpose. The parameter Δz of the Husimi function, i. e., the depth scale of a Gaussian wavepacket, a wavefield is projected to, is taken of 100 m.

1. $\lambda_z = 2000$ m

We begin with considering the sound-speed inhomogeneity with $\lambda_z = 2000$ m. Fig. 2 represents the matrices of absolute values of C_{mn} calculated with the frequencies of 20 Hz (a), 50 Hz (b), 100 Hz (c), and 200 Hz (d). In the case of $f = 20$ Hz, the elements along the main diagonal have the values close to 1, while other ones are near zero. It means that the perturbation doesn't cause significant mode coupling, and each Floquet mode consists of only one mode of the unperturbed waveguide. All the ray-based predictions fail. As f increases, the situation becomes more complicated. In the case of $f = 50$ Hz, the diagonal elements still dominate, but an additional pair of parallel stripes appears in two blocks of the matrix $\|C_{mn}\|$. The vertical spacings between stripes and the main diagonal are equal to 9 in the center block and 10 in the right lower one. It corresponds to the order of dominant ray-medium resonance. The presence of those stripes is the manifestation of the so-called mode-medium resonances [9, 14] being the wave-based analogues of quantum nonlinear resonances [15].

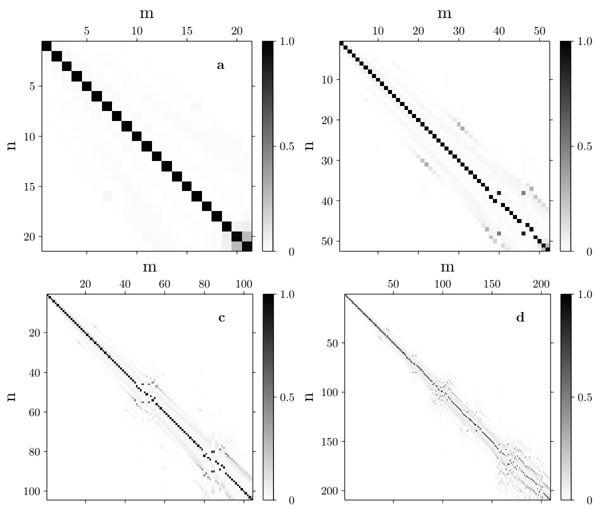

Fig. 2. Absolute values of the coefficients C_{mn} determining decomposition of the Floquet modes over modes of the unperturbed waveguide. The vertical wavelength of the sound-speed perturbation λ_z is 2000 m. Acoustic frequency is 20 Hz (a), 50 Hz (b), 100 Hz (c), and 200 Hz (d)

The triplets bear smeared patterns that look like "dial-plates" on the Husimi plots of the respective Floquet modes. Examples of such "dial-plates" are shown in Figs. 3(a) and (b). The ray-medium resonance 8 : 1 (corresponding to the block in the upper left corner of the matrix) appears too narrow to form the triplet structure with the frequency of 50 Hz, but with larger frequencies, 100 and 200 Hz, a weak triplet occurs (in the upper left corners of the matrices). Besides that, in the cases of higher frequencies, the triplets corresponding to the resonances 9 : 1 or 10 : 1 transform into multiplets, which are somewhat distorted, probably due to the lack of the procedure of numbering the Floquet modes.

In a sharp contrast to the triplets, the multiplets give rise to well-resolved peaks on the Husimi plots (see Figs. 3(c)–(e)). These peaks arise on the stable or unstable periodic orbits of ray-medium resonances. Floquet modes, belonging to the chaotic layer, are spread as it is shown in Fig. 3(f) but also have regular structure.

Thus, the case of a slowly depth-oscillating sound-speed perturbation reveals similar patterns as those occurring in the absence of depth oscillations [14]. One peculiarity we should emphasize

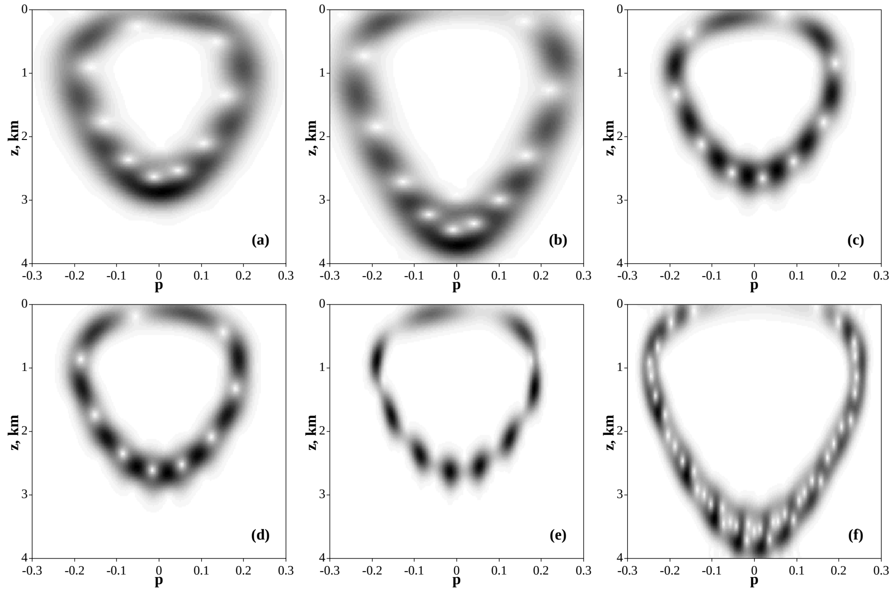

Fig. 3. Examples of Floquet modes computed with $\lambda_z = 2000$ m and illustrated via the Husimi plots. (a) $f = 50$ Hz, $m = 31$, (b) $f = 50$ Hz, $m = 46$, (c) $f = 100$ Hz, $m = 49$, (d) $f = 100$ Hz, $m = 52$, (e) $f = 200$ Hz, $m = 101$, (f) $f = 200$ Hz, $m = 189$

is that mode-medium resonances corresponding to ray-medium resonances of different orders form multiplets in certain blocks of the matrix $\|C_{mn}\|$, and those blocks are well separated from each other.

2. $\lambda_z = 1000$ m

Now let's proceed with the case of $\lambda_z = 1000$ m. As we saw above, the essential features of the respective Poincaré map are the prominent ray-medium resonance $8:1$ and the wide chaotic sea corresponding to steep rays and, according to the ray-mode duality, high-number modes. The matrix $\|C_{mn}\|$ is presented in Fig. 4. Note that there is no such a salient dominance of the main diagonal as in the previous case, and mode coupling is significantly stronger. Remarkable triplet pattern appears even with $f = 20$ Hz. Owing to that, some of the Floquet modes computed with $f = 20$ Hz reveal a "dial-plate" pattern of the resonance $9:1$, as that is depicted in Fig. 5(a). The matrix with 50 Hz represents an almost ordered multiplet pattern, a part of which transforms into a large fuzzy block with higher frequencies. There arise the modes like the one presented in Fig. 5(b). It consists of distinct peaks of the resonance $8:1$ and expands into the phase space domain corresponding to the chaotic sea. On the ray level, the ray-medium resonance $8:1$ is isolated from the chaotic sea by invariant curves which are impenetrable for rays. Presence of such Floquet modes is a manifestation of the phenomenon *dynamical tunneling* [16, 17] known in the theory of quantum chaos. It means penetration of wave functions through classical phase space barriers. Another feature we should note is the presence of identifiable chain of peaks corresponding to the resonance $9:1$ (see Fig. 5(c)) which is destroyed on the ray level, but its periodic ray orbits do exist and give the contribution into the scarred Floquet modes [18]. Fig. 5(d) illustrates the Floquet mode involving the peaks of resonances $9:1$ and $10:1$, simultaneously.

Thus, decreasing twice the vertical length scale leads to the amplification of mode coupling.

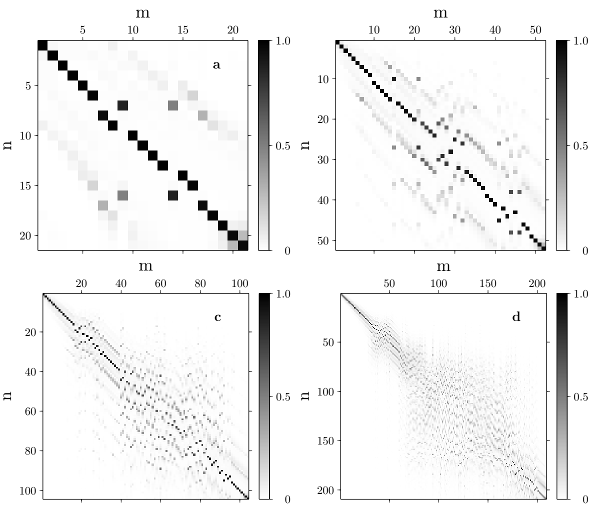

Fig. 4. The same as in Fig. 2 but for $\lambda_z = 1000$ m

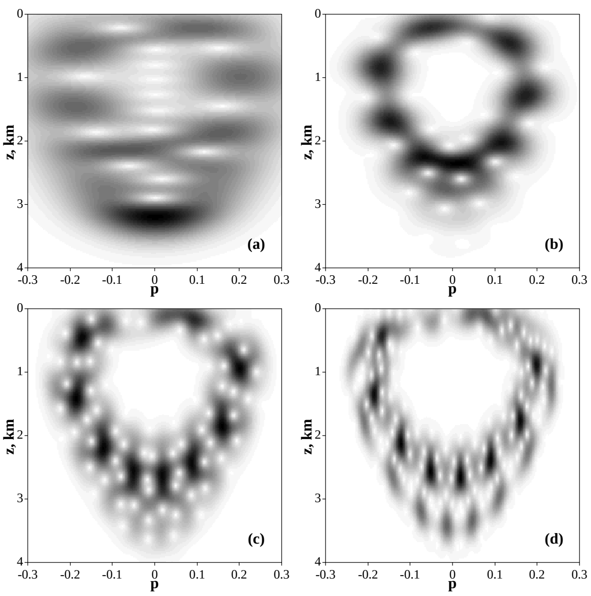

Fig. 5. Examples of Floquet modes computed with $\lambda_z = 1000$ m and illustrated via the Husimi plots. (a) $f = 20$ Hz, $m = 14$, (b) $f = 50$ Hz, $m = 20$, (c) $f = 100$ Hz, $m = 53$, (d) $f = 200$ Hz, $m = 109$

However, the phenomena observed are still well-consistent with the ray-based pattern, except for the tunneling modes. It is not surprising, because the depth oscillations are still very slow, and the short-wavelength approximation still works well.

3. $\lambda_z = 500$ m

A sound-speed perturbation with $\lambda_z = 500$ m induces two separate nested chaotic layers in phase space (see Fig. 1(c)). The wide inner layer is induced by a vertical resonance and contains several chains of islands within. The outer one is significantly smaller. Even with $f = 20$ Hz, the matrix $\|C_{mn}\|$ has a tridiagonal form. With higher frequencies, the matrix has multiplets being drawn along the upper half of the main diagonal, and Floquet modes reveal well-resolved ordered peaks, as well as extended patterns covering the inner chaotic layer (see Fig. 6). Notably,

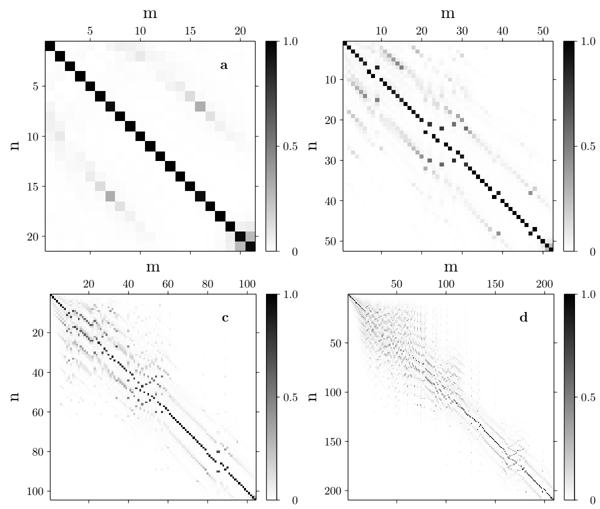

Fig. 6. The same as in Fig. 2 and 4 but for $\lambda_z = 500$ m

the outer chaotic layer appears too narrow and is not reflected significantly in the matrix. We focus our attention at the case of $f = 200$ Hz. The ray-medium resonances 8 : 1 and 9 : 1 are merged into the chaotic sea, but give rise to ordered chains of peaks, attributed to the effect of scarring [18]. Although the resonance 8 : 1 has three chains of stable islands due to the perturbation-induced degeneracy, only one chain of eight peaks is present in the corresponding Floquet modes, one of them is shown in Fig. 7(a). So, the multiplication of periodic orbits is suppressed and the pre-bifurcation state involving only one chain of eight orbits is recovered in the wave pattern. We postpone the discussion of this phenomenon to the next subsection when it will reveal itself more apparently. Notably, the localization of the Floquet modes near its periodic orbits is weaker for the resonance 8 : 1 than for the resonance 9 : 1 (compare Figs. 7(a) and (b)), despite the latter one hasn't undestroyed islands in the ray limit. There are also a family of Floquet modes covering almost entirely the inner chaotic layer. They expose spectacular patterns consisted of several chains of peaks, being well-ordered though. Examples of such Floquet modes are demonstrated in Figs. 7(c)–(e). The Floquet mode depicted in Fig. 7(f) exhibits the effect of dynamical tunneling. It is concentrated predominantly at the stable region, but expands simultaneously over the both inner and outer chaotic layers.

Thus, we can see that features inconsistent with ray-based description tend to grow with decreasing the perturbation wavelength λ_z. In addition to the dynamical tunneling, here we encountered the nontrivial effect of suppression of the bifurcation leading to multiplication of the orbits of the resonance 8 : 1.

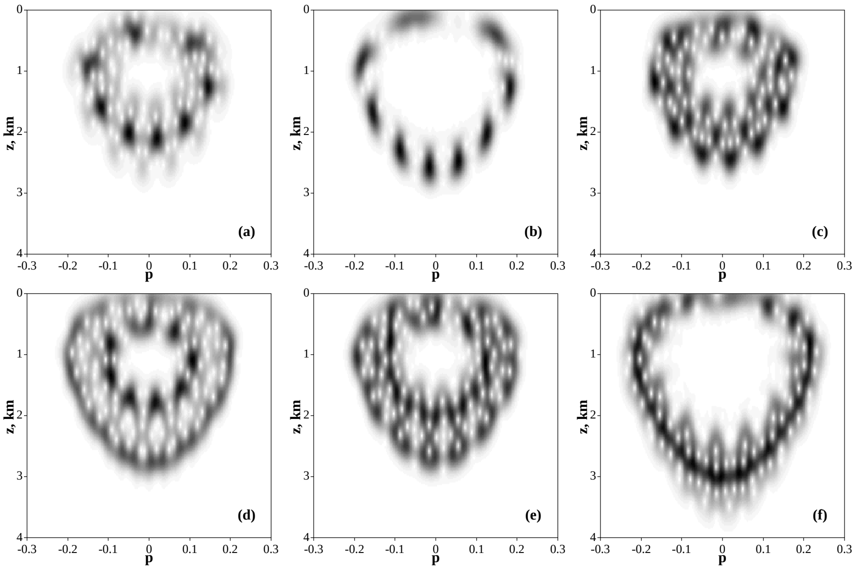

Fig. 7. Examples of Floquet modes computed with $\lambda_z = 500$ m and illustrated via the Husimi plots. (a) $f = 20$ Hz, $m = 16$, (b) $f = 200$ Hz, $m = 57$, (c) $f = 200$ Hz, $m = 96$, (d) $f = 200$ Hz, $m = 65$, (e) $f = 200$ Hz, $m = 75$, (f) $f = 200$ Hz, $m = 138$

4. $\lambda_z = 200$ m

In the case of $\lambda_z = 200$ m, the wide chaotic sea induced by vertical resonance occupies the central domain of phase space, corresponding to near-axial rays. It should lead to a multiplet pattern in the upper left corner of the matrix $||C_{mn}||$, which corresponds to the Floquet modes propagating near the waveguide axis. This expectation is fulfilled with the frequencies in the range 50–100 Hz, but fails with 20 Hz (see Fig. 8), when the main diagonal is dominant, i. e. modes are decoupled.

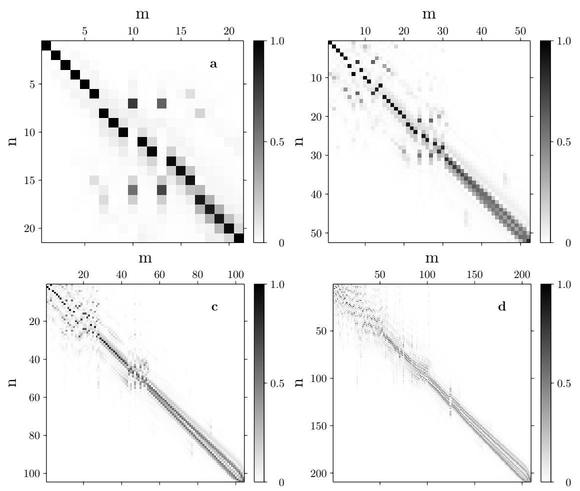

Fig. 8. The same as in Fig. 2, 4 and 6 but for $\lambda_z = 200$ m

At the frequencies of 100 and 200 Hz, the chaotic sea gives rise to widespread Floquet modes like those shown in Figs. 9(a) and (b). These modes are responsible for rapid broadening of a wavepacket until all the chaotic sea will be covered. This regime is well-consistent with the ray limit anticipating rapid spreading and entanglement of any wavepacket belonging to the chaotic sea. With lower frequencies this effect is suppressed or completely disappears.

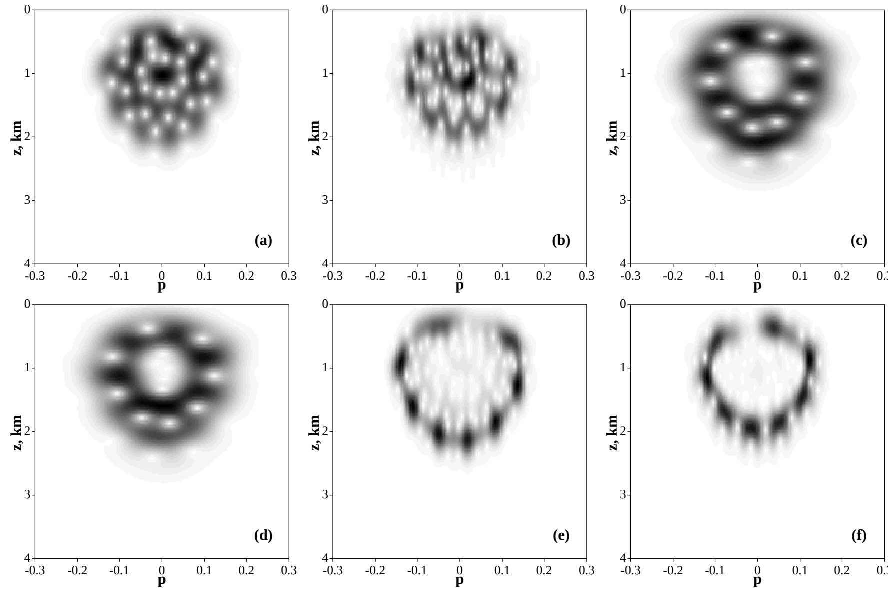

Fig. 9. Examples of Floquet modes computed with $\lambda_z = 200$ m and illustrated via the Husimi plots. (a) $f = 100$ Hz, $m = 11$, (b) $f = 200$ Hz, $m = 24$, (c) $f = 50$ Hz, $m = 12$, (d) $f = 50$ Hz, $m = 8$, (e) $f = 200$ Hz, $m = 57$, (f) $f = 200$ Hz, $m = 47$

We want to pay attention to the following phenomenon. Many of Floquet modes belonging to the chaotic sea have the form as shown in Figs. 9(c)–(f), i. e. they exhibit a chain of eight well-ordered intensity peaks. The peaks with 50 Hz look as the aforementioned "dial-plates". The chains are placed in the area where one should expect the ray-medium resonance 8 : 1, therefore, they should be associated with its periodic ray orbits. If it is true, the peaks in Figs. 9(c) and (e) should correspond to elliptic (center) orbits of the resonance, and the peaks in Figs. 9(d) and (f) to the hyperbolic (saddle) ones. According to the Poincaré map shown in Fig. 1(d), all these orbits are unstable, therefore, the occurrence of the peaks should be attributed to the scarring effect. To verify this suggestion, we compute all periodic orbits of the period $8\lambda_r = 40$ km. Fig. 10(a) indicates that there are a lot of such orbits, and they are distributed very irregularly. However, it should be taken into account that a contribution of any periodic orbit depends on its stability [19]. In Fig. 10(b), we distinguish the most stable periodic orbits and show that locations of eight of them coincide with the locations of the Floquet peaks. Thus, semiclassical theory, albeit in a somewhat restricted form, appears to be useful even in the presence of small-scale features. There is also an orbit near the center, which is not linked anyway to the resonance 8 : 1, and should be attributed to a specific regime of ray motion in the close vicinity of the channel axis.

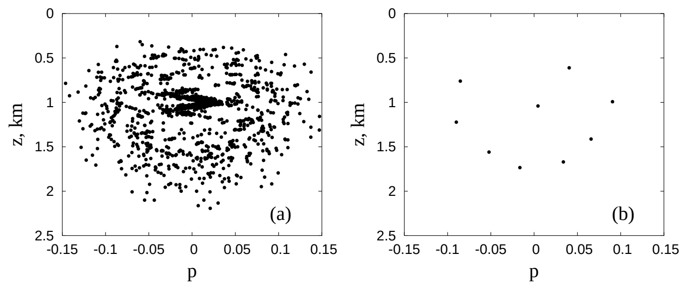

Fig. 10. Locations of periodic orbits in phase space: (a) all periodic orbits of the period $8\lambda_r = 40$ km, (b) the most stable of them

Summary

To summarize, it should be noted that decreasing of λ_z enhances mode coupling that agrees with ray-based predictions. Floquet modes reflect the main features of ray dynamics, such as ray-medium resonances or chaotic layers if the phase space volume of these features is large compared with the unit cell volume k_0^{-1}. Sound speed perturbation with fine-scale oscillations causes bifurcations of periodic orbits which appear irrelevant for wave dynamics because they don't alter regular distribution of the most stable orbits. Therefore, a wavefield recovers the pattern destroyed by the bifurcation. It is also should be noted that the Floquet modes with $f = 20$ Hz are very weakly sensitive to peculiarities of ray dynamics, especially to those induced by rapid depth oscillations of the sound-speed perturbation. It is apparent in the case of $\lambda_z = 200$ m. Although the presence of the wide chaotic sea anticipates strong interaction between low modes, the matrix of the Floquet coefficients $\|C_{mn}\|$ indicates their decoupling.

Authors are grateful to Steven Tomsovic for helpful comments. This work is supported by the joint grant from the Russian Foundation for Basic Research and the Far-Eastern Branch of the Russian Academy of Sciences (project 09-05-98608), the grants from the Prezident of the Russian Federation (project MK 4324-2009.5), and the "Dynasty" Foundation.

References

[1] W.M. Ewing, J.L. Worcel, Long-range sound transmission, *Geol. Soc. Amer. Mem.*, **27**(1948), Pt. 3, 1–32.

[2] L.M. Brekhovskikh, *Dokl. Akad. Nauk SSSR*, **69**(1949), 157 (in Russian).

[3] L.D. Rosenberg, *Dokl. Akad. Nauk SSSR*, **69**(1949), 175 (in Russian).

[4] L.E. Kon'kov, D.V. Makarov, E.V. Sosedko, M.Yu. Uleysky, Recovery of ordered periodic orbits with increasing wavelength for sound propagation in a range-dependent waveguide, *Phys. Rev. E*, **76**(2007), 056212.

[5] D.V. Makarov, L.E. Kon'kov, M.Yu. Uleysky, The ray-wave correspondence and the suppression of chaos in long-range sound propagation in the ocean, *Acoust. Phys.*, **54**(2008), 382–391.

[6] K.C. Hegewisch, N.R. Cerruti, S. Tomsovic, Ocean acoustic wave propagation and ray method correspondence: internal wave fine structure, *J. Acoust. Am. Soc.*, **117**(2005), 1582–1594.

[7] D.V. Makarov, M.Yu. Uleysky, S.V. Prants, Ray chaos and ray clustering in an ocean waveguide, *Chaos*, **14**(2004), 79–95.

[8] D. Makarov, S. Prants, A. Virovlyansky, G. Zaslavsky, Ray and wave chaos in ocean acoustics, Singapore, World Scientific, 2010.

[9] A.L. Virovlyansky, G.M. Zaslavsky, Wave chaos in terms of normal modes, *Phys. Rev. E*, **59**(1999), 1656–1668.

[10] I. Smirnov, A.L. Virovlyansky, G. Zaslavsky, Theory and applications of ray chaos to underwater acoustics, *Phys. Rev. E*, **64**(2001), 036221.

[11] B.V. Chirikov, A universal instability of many-dimensional oscillator systems, *Phys. Rep.*, **52**(1979), 265-379.

[12] D.V. Makarov, M.Yu. Uleysky, Ray escape from a range-dependent underwater sound channel, *Acoust. Phys.*, **53**(2007), 495–502.

[13] F.J. Beron-Vera, M.G. Brown, J.A. Colosi, S. Tomsovic, A.L. Virovlyansky, M.A. Wolfson, G.M. Zaslavsky, Ray dynamics in a long-range acoustic propagation experiment, *J. Acoust. Soc. Am.*, **114**(2003), 1226–1242.

[14] I. Smirnov, A.L. Virovlyansky, M. Edelman, G. Zaslavsky, Chaos-induced intensification of wave scattering, *Phys. Rev. E*, **72**(2005), 026206.

[15] G. Berman, A. Kolovsky, Quantum chaos in interactions of multilevel quantum systems with a coherent radiation field, *Sov. Phys. Usp.*, **35**(1992), 303–326.

[16] S. Tomsovic, D. Ullmo, Chaos-assisted tunneling, *Phys. Rev. E*, **50**(1994), 145-162.

[17] A. Mouchet, C. Eltschka, P. Schlagheck, Influence of classical resonances on chaotic tunneling, *Phys. Rev. E*, **74**(2006), 026211.

[18] E.J. Heller, Bound-state eigenfunctions of classically chaotic Hamiltonian systems: scars of periodic orbits, *Phys. Rev. Lett.*, **53**(1984), 1515-1518.

[19] S. Tomsovic, E.J. Heller, Long-time semiclassical dynamics of chaos: the stadium billiard, *Phys. Rev. E*, **47**(1993), 282-299.

Волновой хаос в подводной акустике

Денис В. Макаров
Леонид Е. Коньков
Михаил Ю. Улейский

Рассматривается задача о дальнем распространении звука в океаническом волноводе. Слабая горизонтальная неоднородность скорости звука порождает хаотическую динамику в лучевом пределе. В реальном океане важную роль в возникновении неустойчивости играют мелкомасштабные глубинные осцилляции возмущения скорости звука. Эти мелкомасштабные осцилляции способны нарушить лучеволновое соответствие. Мы проводим сравнительный анализ лучевой и волновой картин в фазовом пространстве и отслеживаем, как противоречия между ними нарастают с уменьшением масштаба глубинных осцилляций возмущения. Показано, что полуклассическая теория может воспроизводить качественные особенности волновой динамики даже при малых масштабах осцилляций возмущения. Сильный конфликт возникает только на очень низких акустических частотах.

Ключевые слова: лучевой хаос, волновой хаос, квантовый хаос, дальнее распространение звука в океане, периодические орбиты.